A ray+waveform inversion for the potency tensor

Scott Leaney*, Schlumberger GeoSolutions, Houston, US
leaney@slb.com
and
Chris Chapman, Schlumberger Gould Research, Cambridge, UK

Summary

We describe a frequency domain waveform inversion for microseismic source mechanism in anisotropic media that combines the efficiency of ray theory with the accuracy of waveform fitting. Rather than inverting for the moment tensor as described previously (Leaney *et al*., 2011), we invert for the potency tensor. The source potency tensor is the moment tensor contracted with the compliance tensor of the medium local to the source and has several advantages. Firstly, it contains none of the distorting effects of anisotropy, which may alter characteristic source angles and produce false non-double couple components in the moment tensor, even for a pure slip source; secondly, it allows the source to be decomposed in units of volume, rather than moment. In its simplest form, potency tensor inversion remains a linear problem, with the source medium properties absorbed into the strain Green function. Posterior covariances are more closely related to the source parameters of interest, free from anisotropic distortion. We review the method and demonstrate the advantage on a synthetic case.

Introduction

It is well known that anisotropy local to an event can distort source attributes of interest (e.g. Julian *et al*., 1998). Anisotropy can cause non-double components in the moment tensor, even for a pure slip source, and can rotate TNP axes and associated strike, dip and rake angles (e.g. Leaney and Chapman, 2010). These distortions can be obviated by decomposing the potency tensor rather than the moment tensor (Chapman and Leaney, 2012). The term potency tensor was first introduced by Ben-Menahem and Singh (1981) and was subsequently used by Heaton and Heaton (1989) and Ben-Zion (2001) wherein it was argued that it was superior to the moment tensor as a source descriptor as it does not depend on the properties of the medium local to the event. In fact the concept of the potency tensor was essentially contained in much earlier work (e.g. Eshelby, 1957).

Chapman and Leaney (2012) (eq. 86) write the moment tensor as

$$\boldsymbol{M} = [V]\kappa_{emb}\boldsymbol{I} + \tfrac{1}{2}A[d]\boldsymbol{c}\colon(\widehat{\boldsymbol{d}}\widehat{\boldsymbol{n}} + \widehat{\boldsymbol{n}}\widehat{\boldsymbol{d}}), \tag{1}$$

where $[V]$ is the volume change due to an isotropic pressure change in a cavity, $\kappa_{emb}$is the embedded anisotropic bulk modulus, and the second dyadic term describes a moment tensor source due to a displacement discontinuity (DD), across a fracture with unit normal $\widehat{\boldsymbol{n}}$. A is the area on the fracture where displacement of total amount (length) equal to $[d]$ has occurred. The unit displacement vector $\widehat{\boldsymbol{d}}$ need not lie in the plane of the fracture so that both opening and slip are included in the DD source term. Since opening produces an isotropic moment term, if opening is present then the total volume change is split between fracture opening and isotropic pressure change. We note that Vavryčuk (2005) considered focal mechanisms in anisotropic media but omitted the first term in (1).

Chapman and Leaney (2012) (eq. 87) write the potency tensor as

$$\boldsymbol{D} = \boldsymbol{s}:\boldsymbol{M} = [V]\kappa_{emb}\boldsymbol{K} + \tfrac{1}{2}A[d](\widehat{\boldsymbol{d}}\widehat{\boldsymbol{n}} + \widehat{\boldsymbol{n}}\widehat{\boldsymbol{d}}), \tag{2}$$

where $\boldsymbol{s}$ is the compliance tensor, the inverse of the stiffness tensor at the source, and $\boldsymbol{K}$ is the hydrostatic pressure modulus tensor, equal to $\frac{1}{3\lambda+2\mu}\boldsymbol{I}$ in an isotropic medium. Notice that the units of (2) are L^3 or volume. In (2) $[V]$ is the isotropic dilatation or volume change. In an anisotropic medium an isotropic dilatation would require a complicated source mechanism, and while we prefer a source model that admits an isotropic pressure source in a cavity together with a DD source as in (1), to keep the inverse problem linear we presently consider an inversion for the potency tensor source described by equation 2. A hybrid linear+nonlinear inversion for potency tensor and isotropic pressure source will be discussed elsewhere.

In what follows we review the ray+waveform inversion method (Leaney *et al*., 2011) with the modification of inverting for the potency tensor. We illustrate the advantages of a potency tensor inversion by comparing source parameters computed from random perturbations of $\boldsymbol{M}$ and $\boldsymbol{D}$ for a pure slip source in an anisotropic medium.

Theory and Method

Consider far-field vector recordings of particle velocity at angular frequency ω, $\boldsymbol{v}(\omega, \boldsymbol{x}_j, \boldsymbol{x}_s)$, at receiver location $\boldsymbol{x}_j$ for a source at location $\boldsymbol{x}_s$ in terms of the potency tensor $\boldsymbol{D}(\omega)$. In the geometrical ray approximation (Chapman, 2004):

$$\boldsymbol{v}(\omega, \boldsymbol{x}_s, \boldsymbol{x}_j) = r_j(\omega)\{[\textstyle\sum_k^{rays} \widehat{\boldsymbol{g}}_k(\boldsymbol{x}_s, \boldsymbol{x}_j)G_k(\omega, \boldsymbol{x}_s, \boldsymbol{x}_j)\boldsymbol{E}_k : \boldsymbol{c}] : \boldsymbol{D}(\omega)\} \tag{3}$$

where $r_j(\omega)$ is the response of receiver j to displacement signals at $\boldsymbol{x}_j$. In (3) $\widehat{\boldsymbol{g}}_k$ is the polarization vector at the receiver for ray k connecting source and receiver, G_k is the scalar ray propagation term corresponding to the third-order strain Green function, and $\boldsymbol{E}_k = (\widehat{\boldsymbol{p}}\widehat{\boldsymbol{g}} + \widehat{\boldsymbol{g}}\widehat{\boldsymbol{p}})/2$ is the second-order ray strain tensor at the source with $\widehat{\boldsymbol{p}}$ the normalized phase slowness vector and $\widehat{\boldsymbol{g}}$ the polarization vector. The symbol : signifies the scalar product between tensors. $\boldsymbol{c}$ is the elastic stiffness tensor at the source, now grouped with medium-related terms rather than the source. All terms inside the square brackets come from the model and ray tracer. Anisotropy impacts not only the source radiation pattern ($\boldsymbol{E_k}:\boldsymbol{M} = \boldsymbol{E}_k:\boldsymbol{c}:\boldsymbol{D}$) and receiver polarization vector but also the propagation terms hidden inside G – times, spreading and transmission loss, and source and receiver impedance coupling terms. Not shown in (3) is a term for anelastic absorption due to Q. For this a practical approach is adopted, with Q values per layer and ray type (qP, qSv, Sh) rather than a full anisotropic Q treatment. The ray tracer returns the average Q for each ray signature and a Futterman-type absorption-dispersion model is used. The sum over rays may include mode conversions, reflections, internal multiples and head waves in addition to direct arrivals.

By invoking the isomorphism between second rank tensors and vectors, and using the modified Voigt matrix representation for the 4-th rank stiffness tensor, $\boldsymbol{c}$, equation (3) can be written in matrix-vector form as $\boldsymbol{d} = \boldsymbol{G}\boldsymbol{m}$. It is solved at each frequency for the six-vector of potency tensor terms using the generalized inverse, $\boldsymbol{G}^{-g}$, computed using a complex SVD routine. The inversion process can be viewed as vector beam-forming, or least-squares time reversal (Leaney, 2008), yielding the estimated $\boldsymbol{D}(\omega)$, each convolved with its own source function. While the study of different source functions for P and S arrivals is of interest (Eaton *et al*., 2012), we seek a real, frequency-independent potency tensor and a single source function. Constraining all six elements of $\boldsymbol{D}$ to have a common source function is a nonlinear problem, so to avoid this we estimate a single source function from estimated $\boldsymbol{D}(\omega)$ as the

maximum variance signal using complex principal component analysis (e.g. Freire and Ulrych, 1988). A weighted deconvolution using this estimated wavelet then leaves the potency tensor. Sacchi (Pers. Comm. 2008) pointed out the similarity of this to an RTM imaging condition.

While linear inverse theory provides a way to calculate uncertainties in estimated parameters, posterior uncertainties in the elements of $\boldsymbol{D}$ (or $\boldsymbol{M}$) are of little use as for source interpretation we are interested in the uncertainties in derived parameters such as the amount of slip and opening, strike and dip angles, etc. These parameters are derived from the eigen analysis of the second rank tensors and while error propagation is possible (Han *et al*., 2007) here we adopt a Monte Carlo approach to study posterior uncertainties using the posterior covariance matrix from linear inverse theory. The covariance matrix for the estimated elements of $\boldsymbol{D}$ (or $\boldsymbol{M}$) is given, in its simplest form for a diagonal data covariance matrix (e.g. Aster *et al*. 2005, eq 4.56) , by

$$\boldsymbol{C}_m = \sigma_d^2[\boldsymbol{G}^T\boldsymbol{G}]^{-1} \tag{4}$$

which can be used to construct multivariate normal random deviates about the maximum likelihood solution honoring the resolving power of the experimental set-up and the noise in the data. Aster *et al*. (2005) in appendix example B.10 provide a recipe for computing a multivariate normal distribution using the Cholesky decomposition of the covariance matrix.

Examples

We illustrate the ideas described in the previous sections via a synthetic example where the source is a pure slip source, the medium is a 1D layered VTI medium and the recording geometry comprises two 12-level vertical arrays. The event location is significantly off the plane defined by the receiver arrays so that all six elements of the moment or potency tensor are resolved; the condition number for this experimental set-up is 18. Equation 3 with an exact layered VTI ray tracer is used for forward modeling. The source function used is a Brune pulse with corner frequency fc=500Hz; velocity geophones are assumed. The source is a pure slip source with potency $A[d] = 10^{-4}m^3$, strike=N20E, dip=40 (plane normal up from horizontal, so plane dipping down to the right looking in the strike direction) and rake=60 (up counter-clockwise from horizontal, meaning predominantly reverse or thrust with a left lateral component). The elastic properties of the medium local to the source are: Vp=4km/s, Vs=2.3km/s, density=2.5gm/cc, e=.33, d=.20, g=.43, a constant Q=100 is used for P, Sh and Sv. An effective isotropic medium can be constructed from the anisotropic moduli using, for example, the mean-squared velocity averaged over all directions (Chapman, 2004, exercise 4.6). For this medium the rms isotropic velocities are Vp=4.63km/s and Vs=2.61km/s. Using this shear velocity in the shear modulus of the medium the moment magnitude of this event is $M_w = -1.9$.

Figure 1 shows P, Sh and Sv radiation patterns ($\boldsymbol{E}_k : \boldsymbol{c} : \boldsymbol{D}$) computed versus phase angle for the pure slip source described above in the anisotropic medium and isotropic medium. Amplitudes are displayed on the upper hemisphere in equal area so that vertical Up is in the center and horizontal is around the edges of the circle. A conventional isotropic moment tensor inversion would assume the radiation patterns shown on the bottom row; our potency tensor inversion accounts for the distortion due to anisotropy, allowing for the correct recovery of source geometry free from anisotropic distortion.

Figure 2 shows synthetic ENU (East, North, Up) waveforms with additive Gaussian noise with standard deviation equal to .05 times the maximum amplitude. The particle velocity signal plus noise was bandlimited to 3-800Hz. The reconstructed ENU data are shown after inversion for the potency tensor and source function. The time domain source function is shown in the right-most panel, and as it is recovered at t0 by the time reversal inversion it has been shifted to the minimum P arrival time for display.

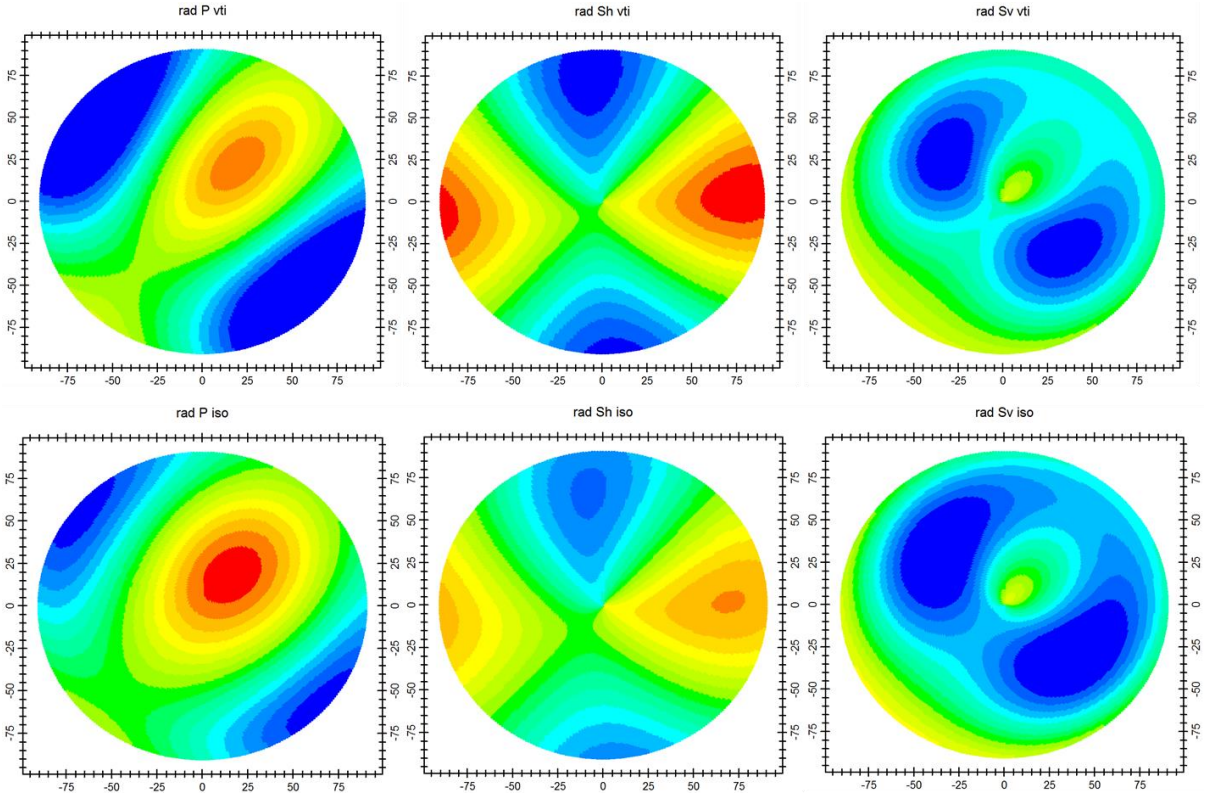

Figure 1: Upper hemisphere equal area P, Sh, Sv (left to right) radiation patterns in an anisotropic (VTI) medium (top row) and in an isotropic medium (bottom row) for the same slip source with equal potency.

For real data, several additional processes are needed. First, since this is waveform inversion, the model must be able to reproduce real data kinematics to within a half-period, with residuals handled by a correlation-based direct arrival static computation. Initial model building utilizes sonic and density data smoothed and blocked following a wavelength criterion. VTI model calibration is done using interactive sliders (Woerpel, 2010) and with a linearized inversion (Mizuno *et al*., 2010) incorporating soft rock physics -based constraints or measured sonic anisotropy to drive layer anisotropy. Special attention is given to pick any Sv arrivals visible on perforation shots and include them in velocity model inversion. Finally model validity is checked not only on perforation locations but on moveout reproduction of high SNR events. Once the model is obtained, usable bandwidth is assessed, and noisy receivers are handled either through omission or by data covariance weighting. Optionally an Lp rather than an L2 solution can be sought using iteratively reweighted least-squares.

Having inverted for the potency tensor or moment tensor we study how errors propagate into source parameters, using the covariance matrices to generate tensors from a multivariate normal distribution. For each randomly generated moment or potency tensor model, conventional moment tensor decompositions (e.g. Hudson *et al*., 1989) are applied. Figure 3 shows a modified Hudson crossplot (k vs. –tau) where we have removed the influence of the experimental geometry from the results by using a diagonal covariance matrix. The modifications to the standard Hudson plot are to flip the horizontal axis and to plot parameters on a diamond without the skew (for a detailed discussion of different moment tensor interpretations, see Chapman and Leaney, 2012). For the randomly sampled moment tensors the central (i.e. maximum likelihood) moment tensor is that for a pure slip source in an anisotropic medium, as would be obtained for example from a moment tensor inversion of sufficiently sampled noise-free data. Perturbed versions of this are obtained according to the diagonal covariance

for $\boldsymbol{M}$. For the potency tensor the central point is again that for a pure slip source, as would be obtained from a noise-free potency tensor inversion. Perturbed versions of this are obtained according to a diagonal covariance for $\boldsymbol{D}$. 1000 models are sampled. The $\boldsymbol{M}$ inversion clearly shows the bias to non-DC components due to the anisotropy of the source medium. The $\boldsymbol{D}$ inversion, on the other hand, maintains a distribution in Hudson space that is centered over a pure slip or DC source.

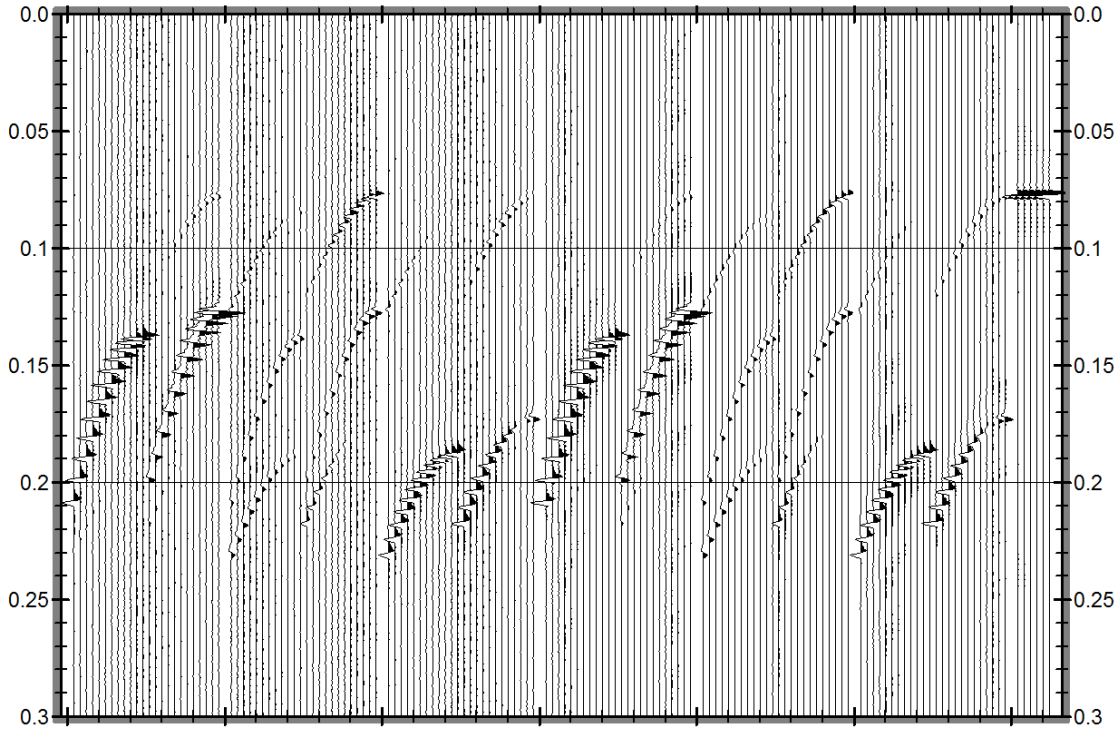

Figure 2: Ray+waveform inversion results for a pure slip source with scalar potency $A[d] = 10^{-4}\text{m}^3$ in a strongly VTI medium. The fracture plane strikes N20E with 40 degrees of dip, the slip vector has a rake of 60. The source function is a Brune pulse with corner frequency fc=500hz. Two twelve level receiver arrays record particle velocities from the far-field displacement signals of the event, having propagated through a layered VTI velocity model with constant Q=100. Thomsen VTI parameters at the event location are ε=.33, δ=.20, γ=.43. Input East, North, Up (ENU) waveforms are shown on the left with additive noise band-limited to 3-800Hz. To the right are reconstructed ENU waveforms after inversion and the estimated source function, shifted from t=0 to the minimum P time and repeated for display.

Figure 4 shows strike, dip and rake angles for the two cases of figure 3, again showing the distortion due to the presence of anisotropy and the advantage of inverting for the potency tensor rather than the moment tensor.

Conclusions

We discuss a modified formulation of the ray+waveform microseismic source inverse problem (Leaney *et al*., 2011) to invert for the potency tensor rather than the moment tensor. In this formulation the source medium stiffness tensor is included in the ray strain Green function, decoupling source parameters from the source medium and leaving only parameters related to source geometry as unknowns. In its simplest form this inverse problem remains linear, like inversion for the moment tensor. We illustrate the advantages of potency tensor inversion by decomposing perturbed moment and potency tensors for a pure slip source where the perturbations honor a posterior covariance matrix. The potency tensor is shown to be superior to the moment tensor in being able to recover the correct source parameters free from the distortion due to anisotropy of the medium containing the source.

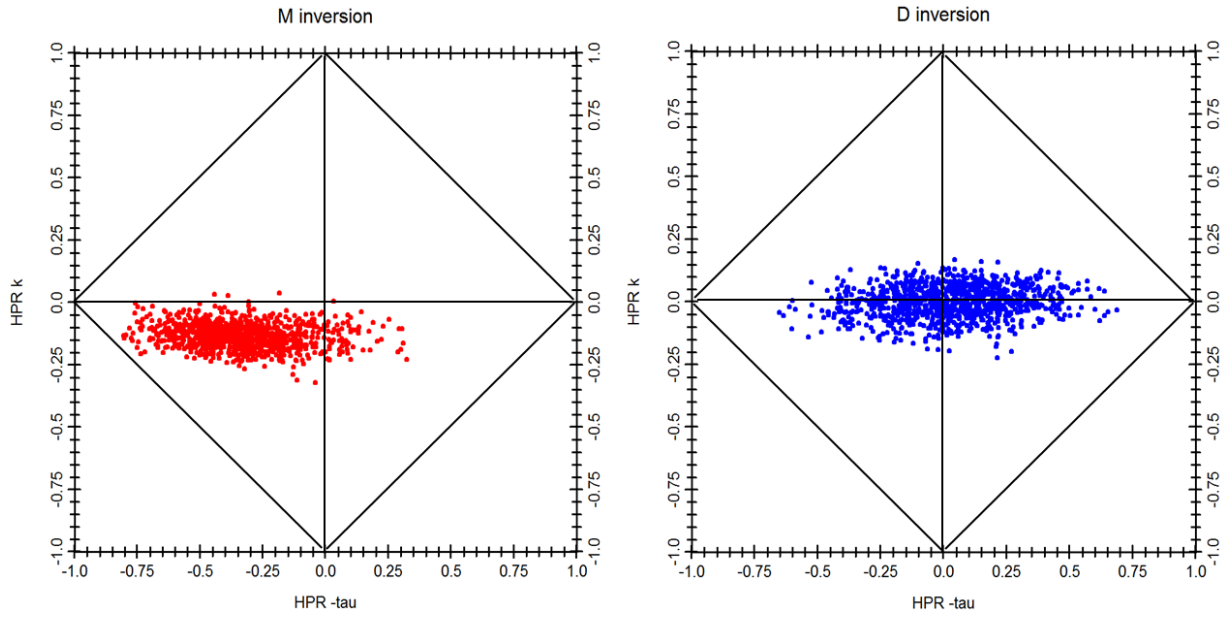

Figure 3: Modified Hudson crossplots (k vs. –tau) for anisotropic moment tensor (left) and potency tensor (right). 1000 multivariate normal realizations are shown for a pure slip source (0,0) using a diagonal covariance matrix with equal variances to remove the influence of the experimental geometry. Potency tensor inversion recovers the source type correctly, free from bias and distortion due to anisotropy.

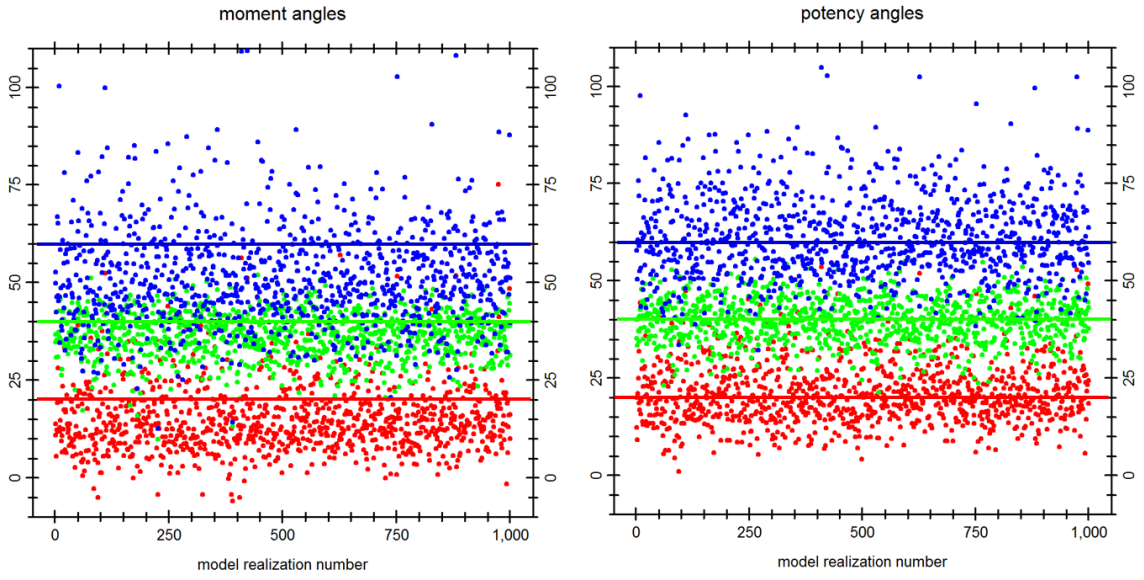

Figure 4: Strike (red), dip (green) and rake (blue) angles for moment tensor (left) and potency tensor (right). Of the dual solutions the one with fracture normal closest to the true fracture normal was chosen. Horizontal lines indicate the true model.

Acknowledgements

Thank you to Professors Tadeusz Ulrych (UBC), Mauricio Sacchi (U of Alberta) and Takashi Mizuno for many helpful discussions.

References

Aster, R.C., Borchers, B. and Thurber, C.H., 2005, *Parameter Estimation and Inverse Problems*, Elsevier.

Ben-Menahem, A. and Singh, S.J., 1981, *Seismic Waves and Sources,* Springer Verlag, New York, NY.

Ben-Zion, Y., 2001, On quantification of the earthquake source, *Seism. Res. Lett.*, **72**, 151-152.

Chapman, C.H., 2004, *Fundamentals of Seismic Wave Propagation*, Cambridge University Press.

Chapman, C.H. and Leaney, W.S., 2012, A new moment tensor decomposition for seismic events in anisotropic media, *Geophys. J. Int. (2012)* ***188****, 343-370.*

Eaton, D.W, van der Baan, M., Birkelo, B. and Tary, J.B., 2012, Scaling relations and spectral characteristics of tensile microseisms, submitted to *Geophysics*.

Eshelby, J.T., 1957, The determination of the elastic field of an ellipsoidal inclusions, and related problems, *Proc. R. Soc. Lond. A.*, **241**, 376-396.

Freire, S.L.M. and Ulrych, T.J., 1988, Application of singular value decomposition to vertical seismic profiling: *Geophysics*, **53**, 778.

Han, J.Y., van Gelder, B.H.W. and Soler, T., 2007, On covariance propagation of eigenparameters of symmetric n-D tensors, *Geophys. J. Int.,* **170**, 503-510.

Heaton, T.H. and Heaton, R.E., 1989, Static deformation from point forces and force couples located in welded elastic Poissonian half-spaces: implications for seismic moment tensors, *Bull. Seism. Soc. Am.*, **79**, 813-841.

Hudson, J.A., Pearce, R.G. and Rogers, R.M., 1989, Source type plot for inversion of the moment tensor, *J. Geophys. Res.*, **94**, 765-774.

Julian, B.R., Miller A.D. and Foulger, G.R., 1998, Non-double-couple earthquakes, 1. Theory, *Rev. Geophys.*, **36**, 525-549.

Leaney, W.S., 2008, Inversion of microseismic data by least-squares time reversal and waveform fitting, SEG Expanded Abstracts, **27**, 1347-1351.

Leaney, W.S. and Chapman, C.H., 2010, Microseismic sources in anisotropic media, 72nd EAGE Extended Abstracts.

Leaney, W.S., Chapman C.H. and Ulrych, T.J, 2011, Microseismic source inversion in anisotropic media, CSEG Expanded Abstracts.

Mizuno, T., Leaney, S. and Michaud, G., 2010, Anisotropic velocity model inversion for imaging the microseismic cloud: 72nd Annual EAGE Conference & Exhibition.

Vavryčuk, V., 2005, Focal mechanisms in anisotropic media, *Geophys. J. Int.*, **161**, 334-346.

Woerpel, C., 2010, Anisotropic velocity modeling for microseismic processing: Part 2 – Fast and accurate model calibration using a cross-well source, SEG Technical Program Expanded Abstracts, 2135-2139.